Assessment of a Multi-Sensor Approach for Noise Removal on Landsat-8 OLI Time Series Using CBERS-4 MUX Data to Improve Crop Classification Based on Phenological Features

Hugo N. Bendini[1], Leila M. G. Fonseca[2], Thales S. Körting[2], Rennan F. B. Marujo[2], Ieda D. Sanches[1], Jeferson S. Arcanjo[2]

[1]Divisão de Sensoriamento Remoto – Instituto Nacional de Pesquisas Espaciais (INPE)

[2]Divisão de Processamento de Imagens – INPE

Caixa Postal 515 – 12.227-010 – São José dos Campos – SP – Brazil

hbendini@dsr.inpe.br, {leila.fonseca,thales.korting, ieda.sanches} @inpe.br, jeferson@dpi.inpe.br

Abstract. *We investigated a method for noise removal on Landsat-8 OLI time-series using CBERS-4 MUX data to improve crop classification. An algorithm was built to look to the nearest MUX image for each Landsat image, based on user defined time span. The algorithm checks for cloud contaminated pixels on the Landsat time series using Fmask and replaces them with CBERS-4 MUX to build the integrated time series (Landsat-8 OLI+CBERS-4 MUX). Phenological features were extracted from the time series samples for each method (EVI and NDVI original time series and multi-sensor time series, with and without filtering) and subjected to data mining using Random Forest classification. In general, we observed a slight increase in the classification accuracy when using the proposed method. The best result was observed with the EVI integrated filtered time series (78%), followed by the filtered Landsat EVI time series (76%).*

1. Introduction

Given the large availability of arable land, and the growing demand for food in the world, Brazil has been consolidated as a big player on the global agricultural scene. Remote sensing is an important tool used within agriculture, regarding its ability to generate information on a large scale in a cost-effective way. In this way, agricultural mapping has become strategic enabling to provide better understanding of the distribution of croplands, and its impact on the environment. With advances in data processing and storage technologies as well as the availability of consistent and continuous long-term image series, remote sensing is undergoing a paradigm shift. Time series techniques stand out for allowing seasonal variation accounts of the analyzed target. Although the use of time series for cropland classification has been well explored using MODIS data (Sakamoto et al., 2005; Arvor et al., 2011; Körting, 2012; Risso et al., 2012; Borges & Sano, 2014; Neves et al., 2016), there is still a demand for more detailed maps, which are made possible from time series with finer spatial resolutions, such as Landsat-like images (Zheng et al., 2015; Peña et al., 2015; Pan et al., 2015; Bendini et al., 2016). As the temporal resolution of Landsat-like satellites it is still low (16 days, generally), an open question in the scientific literature is about how to deal

with the noise in the time series. The noise is characterized by negative outliers, which are possibly a result of factors such as cloud cover, cloud shadow contamination and atmospheric scattering. To deal with this, there are some approaches which include cloud and cloud shadow flags generated from the Automated Cloud Cover Assessment (ACCA) algorithm (Irish et al., 2006) and Fmask algorithm (Zhu & Woodcock, 2012). However, both ACCA and Fmask sometimes fail to detect thin clouds i.e. cirrus and the edges of cumulus clouds (Lymburner et al., 2016) and thus sometimes can be followed by methods based on the use of thresholds (Hamunyela et al., 2013; Bendini et al., 2016; Lymburner et al., 2016) or on the use of smoothers (Pan et al., 2015). There is also the possibility to take advantage of multi-sensor data, considering the large amount of available remote sensing data. In a previous investigation, we show the potential use of higher temporal resolution Landsat-like images for crop mapping (Bendini et al., 2016). Recently the China Brazil Earth Resources Satellite (CBERS) program launched the CBERS-4 that carries in the payload module, among others, the Multispectral Camera (MUX). In this study, we investigated a method for noise removal on Landsat-8 OLI time-series using CBERS-4 MUX data to improve a crop classification method based on phenological features.

2. Materials and Methods

2.1. Study area
The study area is situated in Sao Paulo state (southeast of Brazil), in a region located into the Cerrado biome (Figure 1). As the focus is on croplands, we selected a region of interest where main land cover is agriculture, silviculture and pasture. In this region, farmers grow a variety of crops throughout the year. Major field crops in this area are sugarcane, corn, bean, potato, soybean, sugar beet and onions. There is also production of mango, avocado and eucalyptus. Farmers grow crops in double cropping systems and even in triple cropping systems, mainly within the irrigated areas. The usual planting for summer crops occurs from October to December and harvesting from February to April. We also observed the planting of crops in late fall (May – July) and harvesting in the next spring, especially within the irrigated areas.

2.2. Remote Sensing Data
A total of 23 scenes of Landsat-8 OLI (WRS 2 – Worldwide Reference System2, Path/Row 219/75) between August 2015 and August 2016 were processed to Level 1 Terrain Corrected (L1T). These were corrected for atmospheric conditions to identify and mask cloud and cloud shadows by the USGS EROS Science Processing Architecture (ESPA) (DeVries et al. 2015; DeVries et al. 2015a). Landsat-8 data were corrected using L8SR, a newly developed algorithm that takes advantage of some of Landsat-8's new sensor characteristics (U.S. Geological Survey, 2015; Vermote, 2016). Cloud (pixel value 4), cloud shadow (pixel value 2), snow (pixel value 3), water (pixel value 1) and clear (pixel value 0) masks were provided for Landsat-8 data using Cfmask, a C implementation of the Fmask algorithm (Zhu & Woodcock, 2012; Zhu, Wang, & Woodcock, 2015). The CBERS 4 MUX imagery has been provided by the National Institute for Space Research (INPE).
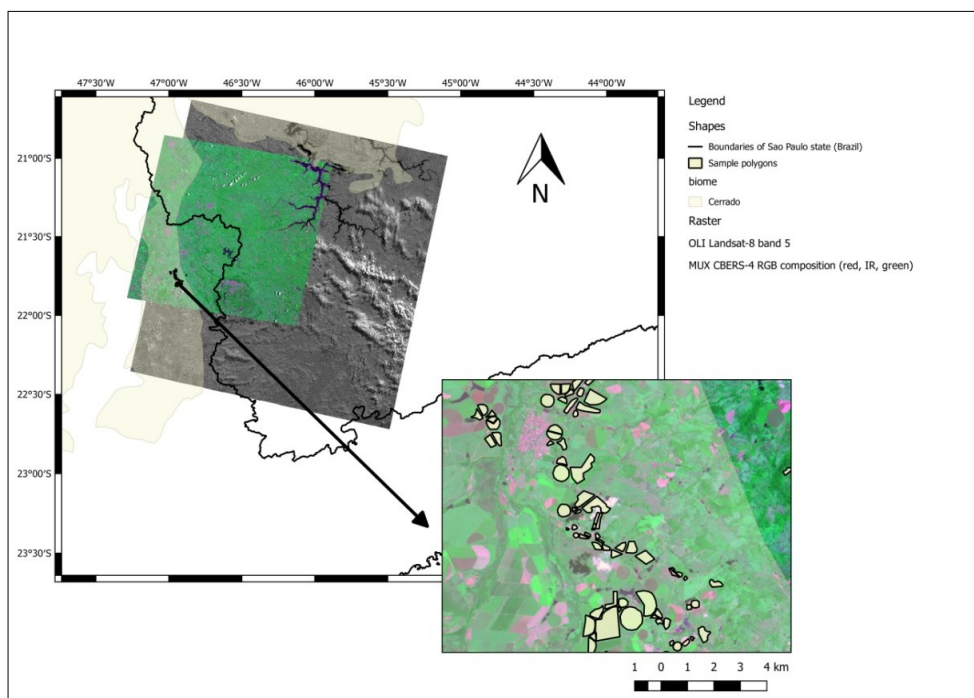
Figure 1. Location of the study area in Sao Paulo state, Brazil.

A total of 11 scenes of CBERS-4 MUX (CBERS WRS Path/Row 155/124) were acquired in the same period (August 2015 and August 2016). They were radiometric and geometrically corrected, adjusted and refined by using control points and the SRTM 30mv. 2.1 digital elevation model (DEM) (Level 4) and corrected for atmospheric conditions using the 6S model (Second Simulation of a Satellite Signal in the Solar Spectrum) (Vermote et al. 1997). Table 1 shows the availability of images from August 2015 to August 2016.

Table 1. Availability of Landsat-8 (Path/Row 219/75) and CBERS-4 (Path/Row 155/124) imagery from August 2015 to August 2016.

Month/Year	Sensor	Acquisition dates (day of year)	Number of scenes
Aug - Dec/2015	OLI	218, 234, 250, 266, 282, 298, 314, 330, 346, 362	10
	MUX	215, 241, 267, 345	4
Jan - Aug/2016	OLI	13, 29, 45, 61, 77, 93, 109, 125, 141, 157, 173, 189, 205, 237	14
	MUX	32, 110, 162, 188, 240	5

For the MUX imagery, we visually assessed the cloud cover for the region of interest for this study. The spectral band specifications for Landsat-8 OLI and CBERS-4 MUX can be seen on Table 2.

Table 2. Spectral band specifications for Landsat-8 OLI and CBERS-4 MUX.

Band	Landsat-8 OLI (µm)	CBERS 4 MUX (µm)
Blue	Band 2: 0.45 - 0.51	Band 5: 0.45 - 0.52
Green	Band 3: 0.53 - 0.59	Band 6 0.52 - 0.59
Red	Band 4: 0.64 - 0.67	Band 7: 0.63 - 0.69
Near Infrared (NIR)	Band 5: 0.85 - 0.88	Band 8: 0.77 - 0.89

The greatest difference in spectral bandwidths between the two sensors are on the NIR band, but there are also significant differences in spectral response function (SRF) profiles between corresponding CBERS-4MUX and Landsat-8 OLI spectral bands (Pinto et al., 2016).
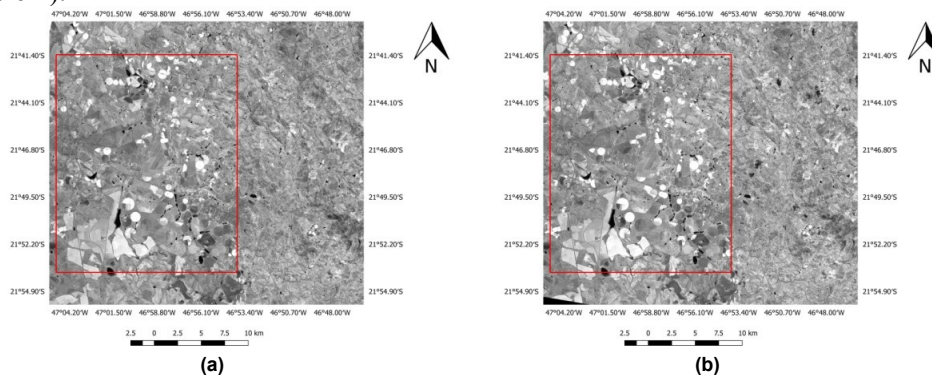
2.3. Correlations Analysis between Landsat-8 OLI and CBERS-4 MUX

First we selected a pair of MUX and OLI images, considering the time proximity between them. The characteristics of the two images are shown in Table 3.

Table 3. Characteristics of the pair of MUX and OLI images used for correlation analysis.

Satellite/Sensor	Date	Acquisition Time (UTC)	Path/Row	Sun elevation	Sun azimuth	Look Angle
CBERS-4 MUX	04 August 2015	13:26:11	155/124	43.37°	36.05°	NADIR
Landsat-8 OLI	06 August 2015	13:03:18	219/75	40.61°	41.58°	NADIR

Considering the difference of spatial resolution between the images (30 meters for OLI and 20 meters for MUX), we resampled the MUX images to 30 meters, using a nearest neighbor approach. To deal with cloud contamination problems, we used the Fmask image to crop a free cloud region on both OLI and MUX surface reflectance images (Figure 2).


Figure 2. Cropped images used on the correlation analysis. (a) Landsat-8 OLI EVI (06 August 2015) and (b) CBERS-4 MUX EVI (August 4th, 2015).

We analyzed the correlations between the cropped images, for each selected vegetation index (EVI and NDVI). In order to determine an equation to predict OLI reflectance from MUX reflectance, linear regressions were constructed.

2.4. Building the multi-sensor time series

An algorithm was built to look to the nearest MUX image for each Landsat image, based on a user defined time span. Here, we used the time span of 8 days. Figure 3 shows a general scheme of the proposed method.
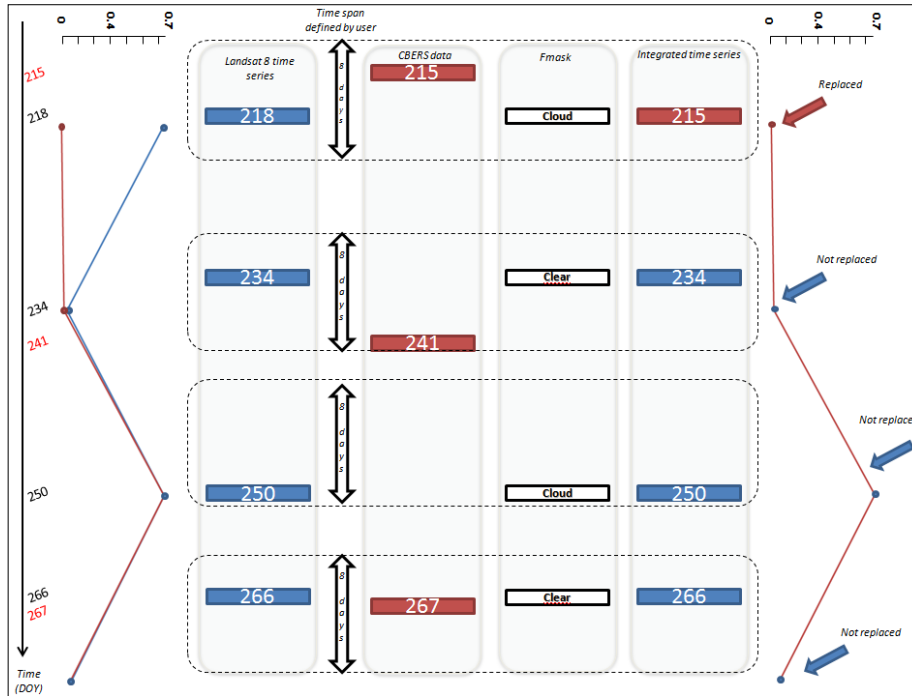
Figure 3. General scheme of the methodology used to build the integrated time series. On the left, a time series of EVI (the red line is the predicted time series using the equation to predict OLI reflectance from MUX and the blue line is the original Landsat time series); on the right is the integrated time series, with marks to illustrate the positions where the replacement has occurred.

After detecting the nearest MUX images for each Landsat images, the algorithm checks for cloud and cloud shadow contaminated pixels on the Landsat time series, by a conditional expression using Fmask images. When a contaminated pixel is detected in the time series, it is replaced by a value calculated from the equation to predict OLI reflectance from MUX, if it is within the time window.

2.5. Filtering the time series

We also applied a combined filtering approach for noise removal on the Landsat time series in order to access the improvement of the classification results compared to the integrated time series. The approach was put forth by interpolating the noise values with the average between the nearest neighbors in time, considering the Fmask quality data (Equation 1) and negative outliers based on a threshold as recommended by Hamunyela et al. (2013) (Equation 2).

$$x_t = \frac{x_{t-1} + x_{t+1}}{2} \{if\ fmask_t = 2\ OR\ fmask_t = 4\} \qquad (1)$$

$$x_t = \frac{x_{t-1} + x_{t+1}}{2} \{if \ x_t - x_{t-1} < -0.01 x_{t-1} \& x_t - x_{t+1} < -0.01 x_{t+1}\} \quad (2)$$

where x_t is an observation of the time series at time t, x_{t-1} is the observation in the time series at time t-1, and x_{t+1} is the observation at time t+1. Observation x_t is replaced as an outlier with the average of x_{t-1} and x_{t+1} if the difference between x_t and x_{t-1} is less than -1% of x_{t-1}, and the difference between x_t and x_{t+1} is less than -1% of x_{t+1}. This method, however, is not capable of removing consecutive outliers. Figure 4 shows an example of how local outliers were removed from the NDVI and EVI time series.
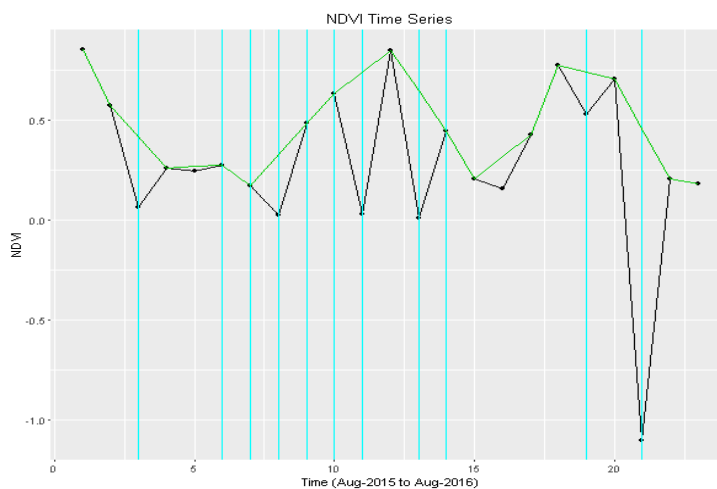

Figure 4. Example of how local outliers were removed from the NDVI time series. The cyan lines are the positions where cloud and cloud shadow were detected by Fmask. The black line is the integrated time series and the green line is the filtered integrated time series using Equation 2.

2.5. Extracting phenological features for classification

We selected 100 well-known polygon samples in the study area, considering the classes of annual agriculture (potato, corn, sugar beet, onion, bean and soybean), perennial agriculture (avocado and mango), semi-perennial agriculture (sugarcane), grassland and native forest.

We extracted NDVI and EVI time series of pixels from each sample polygon in the study area. Phenological metrics in time series were obtained by the TIMESAT v3.2 software (Jönsson; Eklundh, 2004), where seasonal data are extracted for each of the growing seasons of the central year (Figure 5). During a period of n years there may be n – 1 full seasons together with two fractions of a season in the beginning and end of the time series. So, to extract seasonality parameters from one year of data, the time series has been duplicated to span three years, as recommended by Jönsson and Eklundh (2015). For the phenological metrics extraction, the time series was smoothed considering the double logistic filter (Zhang et al., 2003; Jönsson; Eklundh, 2004). This function is recommended for smoothing image time series on cropland areas in the Brazilian Cerrado (Borges & Sano, 2014).

Figure 5 illustrates the schema of the seasonality parameters generated by TIMESAT. In this study, we assume that the seasonality parameters are the same of the phenological metrics. The time for the beginning of season (a), or start of the season (sos), and the end of season (eos) (b) is the time for which the left and right edge, respectively, has increased to a defined level (often a certain fraction of the seasonal amplitude) measured from the minimum level on the corresponding side. The length of the season (c) is the time from the start to the end of the season. Base value (d) is given as the average of the left and right minimum values. The middle of season (e) is computed as the mean value of the times for which, respectively, the left edge has increased to the 80 % level and the right edge has decreased to the 80 % level.
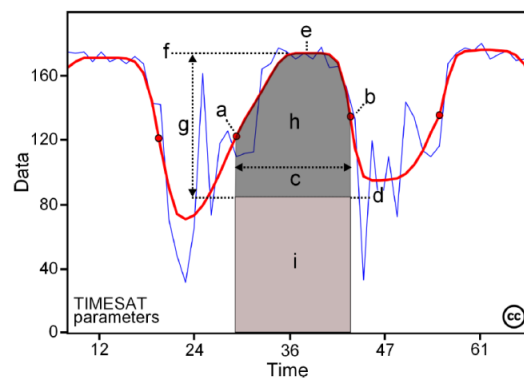
Figure 5. Some of the seasonality parameters generated by TIMESAT: (a) beginning of season, (b) end of season, (c) length of season, (d) base value, (e) time of middle of season, (f) maximum value, (g) amplitude, (h) small integrated value, (h+i) large integrated value. The red and blue lines represent the filtered and the original data, respectively.

The maximum value (f), or the peak of the phenological cycle, is the largest data value for the fitted function during the season. The seasonal amplitude (g) is the difference between the maximum value and the base level. The left derivative is calculated as the ratio of the difference between the left 20% and 80% levels and the corresponding time difference. The right derivative (i.e. the rate of decrease at the end of the season) is the absolute value of the ratio of the difference between the right 20% and 80% levels and the corresponding time difference. The rate of decrease is thus given as a positive quantity. Large seasonal integral (h+i) is integral of the function describing the season from start to end. The small seasonal integral (h) is the integral of the difference between the function describing the season and the base level from start to end of the season (Jönsson and Eklundh, 2015). For more details see Jönsson and Eklundh (2002; 2004).

We subject the phenological metrics obtained on TIMESAT to data mining using the Random Forest (RF) algorithm (Breiman, 2001) considering each method:1) Original Landsat EVI time series; 2) Filtered Landsat EVI time series; 3) Integrated EVI time series; 4) Filtered Integrated EVI time series; 5) Original Landsat NDVI time series, 6) Filtered Landsat NDVI time series, 7) Integrated NDVI time series and 8) Filtered

Integrated NDVI time series. This RF algorithm is a classification technique in which the data set is randomly divided into several subsets of smaller size by means of applying bootstrap, and from each subset a decision tree is developed. All trees contribute to the classification of the object under study, by voting on which class the target attribute must belong. Random Forest algorithm has been widely used in remote sensing (Müller et al, 2015; Peña et al, 2015) because of its advantages in efficiently handling large databases, providing estimates on the most relevant variables, and allowing the identification of outliers (Rodriguez-Galiano et al., 2012). There were a total of 31 training pixels for the annual agriculture classes, 15 pixels for perennial agriculture class, 26 pixels for semi-perennial agriculture, 14 pixels for grassland class and 14 pixels for native forest. The results were evaluated by the confusion matrix index, global accuracy (Witten; Frank; Hall, 2011). The models were executed considering a 10-fold cross validation method. The classification results were obtained using the software package WEKA (Hall et al., 2009).

3. Results and Discussion

The results of the correlation analysis between the cropped images are shown in Figure 6, for each selected vegetation index: a) EVI and b) NDVI.

(a)   **(b)**
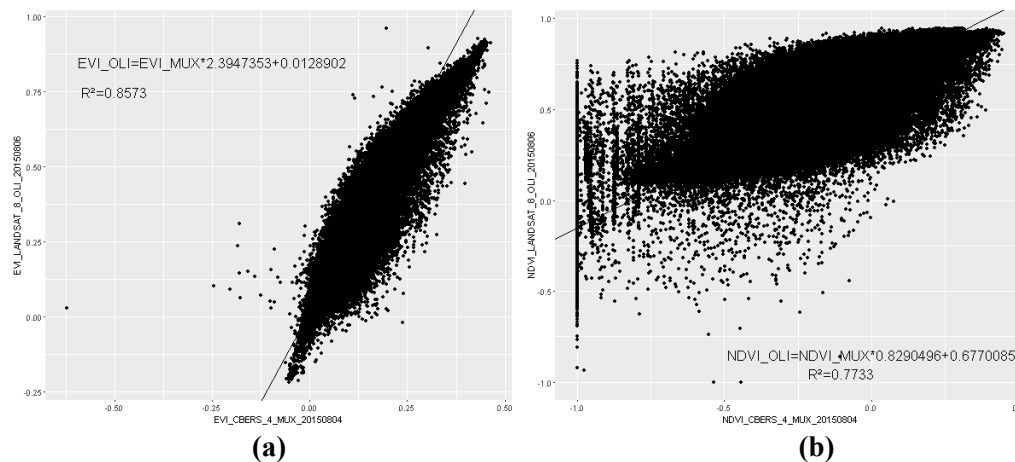
Figure 6. Scatterplot of the pair of cropped images used to determine the linear regressions equations to predict OLI reflectance from MUX reflectance. (a) EVI and (b) NDVI.

The linear regressions equations to predict OLI reflectance from MUX reflectance are also shown. The regression coefficients for EVI and NDVI are respectively 0.8573 and 0.7733. Figure 7 shows the results of different approaches for noise removal on an EVI time series.
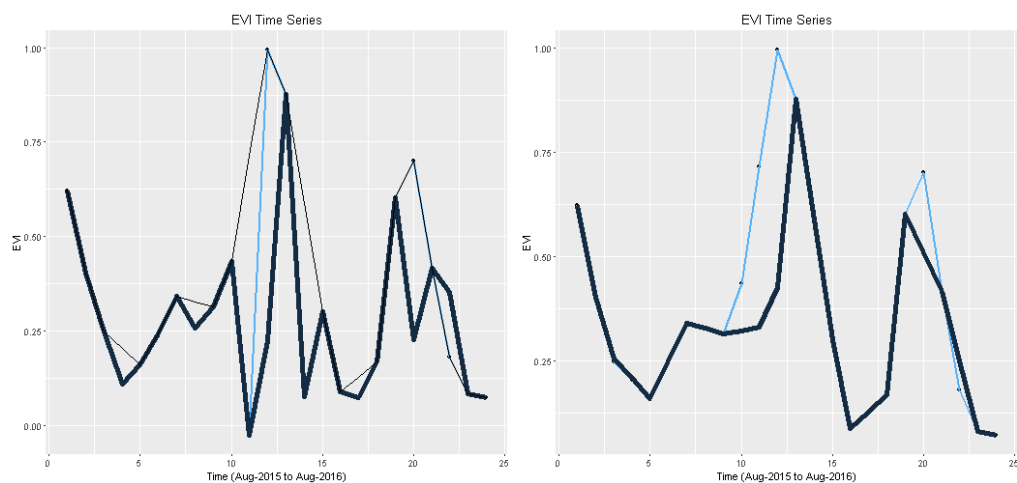
Figure 7. Results of different approaches for noise removal on an EVI time series. On the left the black line is the original Landsat-8 time series, the blue line is the integrated time series and the black thin line is filtered integrated time series. On the right, the blue line is the filtered integrated and the black line is the Landsat-8 filtered time series.

As we can see in Figure 7, the integrated time series can deal with noise, replacing cloud and cloud shadow contaminated pixels withclear pixels of MUX images, and allowing improvement of the time series according to the phenological behavior of the vegetation, which is significant regarding the capability of TIMESAT on extracting the features. We found that concerning the 100 analysed pixels time series, an average of 11.96% of cloud and cloud shadow contaminated observations were replaced using CBERS-4MUX images.

A 10 fold cross-validation technique was applied within the different training sets (Original Landsat EVI time series; Filtered Landsat EVI time series; Integrated EVI time series; Filtered Integrated EVI time series; Original Landsat NDVI time series, Filtered Landsat NDVI time series, Integrated NDVI time series and Filtered Integrated NDVI time series). The accuracy of the different data set classifications are presented in Table 4.

Table 4. Accuracy of classification for the different data set classifications.

Time series Data sets	NDVI	EVI
Integrated	68%	73%
Filtered Integrated	64%	78%
Filtered Landsat	70%	76%
Original Landsat	60%	70%

We found that concerning the NDVI time series, the multi-sensor approach accuracy was 64% when combined with the filtering approach (Equation 2), against 68% without the filtering step. When using only Landsat-8 data, the accuracy was 60%. But when combining the filtering approaches of Equation 1 and 2, the accuracy of the classification results with Landsat-8 time series was 70%.

The results using the EVI time series showed that when the multi-sensor approach was used, the accuracy was higher than when using the original Landsat-8 time series (respectively, 73% and 70%), as well as when combined to the filtering approaches. The classification accuracy using the filtered integrated time series was better than using the Landsat-8 time series (respectively, 78% and 76%). The best result was observed with the filtered integrated EVI time series.

We can derive a hypothesis by that which was observed by Holden et al. (2016), whereby the effect of combining data from the two sensors (L7 ETM+ and L8 OLI), once L7 ETM+ has the same spectral bandwidths of CBERS-4 MUX. NDVI relies on the contrasting relationship between the near infrared band and the red band. They observed that there is a strong and consistent positive bias in NDVI, with Landsat-8 having much higher NDVI. The EVI differs from NDVI by utilizing the blue band as an additional normalizing factor that corrects the red band for atmospheric influences. It appears that the bias in the blue band between Landsat-8 and Landsat-7 nullifies the bias in the red and near infrared band, resulting in a similar EVI across sensors (Holden et al., 2016).This is probably the reason explaining why the results with EVI, when using the integrated time series are better. We can see that small differences on the time series values leads to changes in the results of the smoothers improved by TIMESAT. Furthermore, differences on the extracted parameters can modify the results of classification. As the MUX NDVI values tend to be higher, it modifies the amplitude of the signal, resulting in significant changes on the smooth time series. We can also see in Figure 6 that the regression coefficient between the Landsat NDVI and MUX NDVI are significantly lower than in respect EVI. As observed by Pinto et al. (2016), the greatest difference in spectral bandwidths between the sensors are on the NIR band, but there are also significant differences in SRF profiles between corresponding CBERS-4MUX and Landsat-8 OLI spectral bands (Pinto et al., 2016).

Thus, we can suggest that normalizing the SRF between the sensors would improve the results. We can also infer that the different methods of atmospheric correction may be affecting the results; as well problems of misregistration between the images and resampling can also be a source of errors. More studies are needed to better comprehend the effects of the different filtering approaches, as well to understanding these effects on the smooth improved by TIMESAT with double logistic functions. It is also suggested to test the other smooth approaches implemented by TIMESAT as the Asymmetric Gaussian functions and Savitzky-Golay.

5. Acknowledgements

References

Arvor, D., Jonathan, M., Meirelles, M. S. O. P., Dubreuil, V., Durieux, L., 2011. Classification of MODIS EVI time-series for crop mapping in the state of Mato Grosso, Brazil. International Journal of Remote Sensing, 32 (22), pp. 7847-7871.

Bendini, H., Sanches, I. D., Körting, T. S., Fonseca, L. M. G., Luiz, A. J. B., and Formaggio, A. R.: Using Landsat 8 Image Time Series For Crop Mapping In A Region Of Cerrado, Brazil, Int. Arch. Photogramm. Remote Sens. Spatial Inf. Sci., XLI-B8, 845-850, doi:10.5194/isprs-archives-XLI-B8-845-2016, 2016.

Borges, E.F., Sano, E. E., 2014. Séries temporais de EVI do MODIS para o mapeamento de uso e cobertura vegetal do oeste da Bahia. Boletim de CiênciasGeodésicas, 20 (3), pp. 526-547.

Breiman, L., 2001. Random Forests.Machine Learning. Vol 45, pp. 5-32.

Hall, M. A.; Frank, E.; Holmes, G.; Pfahringer, B.; Reutemann, P.; Witten, I. H.2009. The WEKA Data Mining Software: An Update; SIGKDD Explorations. New York, v.11, n.1, p. 10-18.

Hamunyela, E., Verbesselt, J., Roerink, G., &Herold,M. (2013). Trends in spring phenology ofWestern European deciduous forests.Remote Sensing, 5(12), 6159–6179 http://doi.org/10.3390/rs5126159.

Holden, E. C., Curtis, E. W., (in press) 2016.An analysis of Landsat 7 and Landsat 8 underflight data and the implications for time series investigations.Remote Sensing of Environment.

Irish, R.R. ,Barker,J.L., Goward, S.N., Arvidson, T. (2006), Characterization of the Landsat-7 ETM +automated cloud-cover assessment (ACCA) algorithm. Photogrammetric Engineering and Remote Sensing, 72, pp. 1179–1188

Jönsson, P., Eklundh, L. 2002. Seasonality extraction by function fitting to time-series of satellite sensor data.IEEE Transactions on Geoscience and Remote Sensing. 40 (8), pp. 1824-1831.

Jönsson, P., Eklundh, L. 2004. TIMESAT – a program for analyzing time-series of satellite sensor data.Computers & Geosciences. 30 (8), pp. 833-845.

Jönsson, P., Eklundh, L., 2015. TIMESAT 3.2 with Parallel Processing Software Manual. Lund University, Sweden. pp. 22-24.

Korting, T. S., 2012. Geodma: A Toolbox Integrating Data Mining with Object-Based and Multi-Temporal Analysis of Satellite Remotely Sensed Imagery. PhD Thesis, National Institute for Space Research (INPE). 97p.

Lymburner, L., et al. (2016), Landsat 8: Providing continuity and increased precision for measuring multi-decadal time series of total suspended matter, Remote Sensing of Environment, http://dx.doi.org/10.1016/j.rse.2016.04.011

Müller, H., Rufin, P., Griffiths, P., Siqueira, A. J. B., Hostert, P., 2015. Mining dense Landsat time-series for separating cropland and pasture in a heterogeneous Brazilian savanna landscape. Remote Sensing of Environment, 156, pp. 490-499.

Neves, A. K., Bendini, H. N., Körting, T. S., Fonseca, L. M. G., (in press) 2016. Combining Time Series Features and Data Mining to Detect Land Cover Patterns: A Case Study in Northern Mato Grosso State, Brazil. Revista Brasileira de Cartografia.

Pan, Z.; Huang, J., Zhou, Q., Wang, L., Cheng, Y., Zhang, H., Blackburn, G. A.; Yan, J., Liu, J., 2015. Mapping crop phenology using NDVI time-series derived from HJ-

1A/B data. International Journal of Applied Earth Observation Geoinformation, 34, pp. 188-197.

Peña, M.A., Brenning, A., 2015. Assessing fruit-tree crop classification from Landsat-8 time-series for the Maipo Valley, Chile. Remote Sensing of Environment, 171, pp. 234-244.

Pinto, C., Ponzoni, F., Castro, R., Leigh, L., Mishra, N., Aaron, D., Helder, D. (2016)First in-Flight Radiometric Calibration of MUX andWFI on-Board CBERS-4.Remote Sens., 8, 405; doi:10.3390/rs8050405

Risso, J.,Rudorff, B. F. T., Adami, M., Aguiar, A. P. D., Freitas, R. M, 2012. MODIS Time Series for Land Use Change Detection in Fields of the Amazon Soy Moratorium. In: International Archives of the Photogrammetry, Remote Sensing and Spatial Information Sciences, Melbourne, Australia, Vol. 23, pp. 339-344.

Rodriguez-Galiano, V. F., Ghimire, B., Rogan, J., Chica-Olmo, M., Rigol-Sanchez, J. P., 2012. An assessment of the effectiveness of a random forest classifier for land-cover classification. ISPRS Journal of Photogrammetry and Remote Sensing, 67, pp. 93-104.

Sakamoto, T., Yokozawa, M., Toritani, T., Shibayama, M., Ishitsuka, N., Ohno, H., 2005.A crop phenology detection method using time-series MODIS data.Remote Sensing of Environment, 96 (3-4), pp. 366-374.

U.S. Geological Survey, 2015.U.S. Geological SurveyPRODUCT GUIDE: Landsat Surface Reflectance products courtesy of the U.S. Geological Survey(2015), pp. 1–27

Vermote, E.; Tanre, D.; Deuze, J.; Herman, M.; Morcette, J.J. (1997).Second simulation of thesatellite signal in the solar spectrum, 6S: An overview. IEEE Trans. Geosci. RemoteSens., 35, 675–686.

Vermote, E. (2016). Placeholder: Landsat 8 surface reflectance correction. Remote Sensing of Environment (PLACEHOLDER (PLACEHOLDER), 0–0).

Witten, I. H.; Frank, E.; Hall, M. A. 2011.Data mining: practical machine learning tools and techniques. 3ed. San Francisco: Morgan Kaufmann.

Zhang, X., Friedl, M. A., Schaaf, C. B., 2003.Monitoring vegetation phenology using MODIS.Remote Sensing of Environment. 84, pp. 471-475.

Zheng, B.; Myint, S. W. Thenkabail, P. S.; Aggarwal, R. M. 2015.A support vector machine to identify irrigated crop types usingtime-series Landsat NDVI data.International Journal of Applied Earth Observation and Geoinformation. 34, pp. 103-112.

Zhu and Woodcock, 2012. Z. Zhu, C.E. Woodcock. Object-based cloud and cloud shadow detection in Landsat imagery. Remote Sensing of Environment, 118 (2012), pp. 83–94 (URL: http://dx.doi.org/10.1016/j.rse.2011.10.028)

Zhu, Z., Wang, S., & Woodcock, C. E. (2015b). Improvement and expansion of the Fmask algorithm: cloud, cloud shadow, and snow detection for Landsats 4–7, 8, and Sentinel 2 images. Remote Sensing of Environment (URL: http://dx.doi.org/10.1016/j.rse.2014. 12.014).